Icarus 388 (2022) 115215

Contents lists available at ScienceDirect

Icarus

journal homepage: www.elsevier.com/locate/icarus

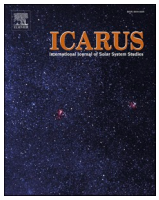

Displacement-length scaling relations of nearside graben: Evidence of restricted normal faults on the Moon

Emily S. Martin *, Thomas R. Watters

Center for Earth and Planetary Studies, National Air and Space Museum, Smithsonian Institution, Washington DC, USA

ARTICLE INFO

Keywords:
Graben
Tectonics
Displacement-length scaling
Normal faults

ABSTRACT

Evidence of significant extension on the Moon is associated with nearside mare. The load induced by the mare basalts resulted in lithospheric flexure and graben forming extension. We use high-resolution topographic and image data from the Lunar Reconnaissance Orbiter (LRO) and the SELenological and ENngineering Explorer (SELENE) to generate detailed fault displacement-length (D/L) scaling observations for graben bounding normal faults. Specifically, we focus on the D_{max}/L relations of graben within three geologic settings: lunar highlands, mare, and mixed highlands-mare terrains. The population scaling factor γ for the measured lunar graben is 4.5×10^{-3} ($n = 50$), falling within the range for terrestrial normal faults. The scatter in the D_{max}/L data for mare graben ($\gamma = 4.9 \times 10^{-3}$, $n = 25$) is significantly higher than that for graben in highlands ($\gamma = 6.3 \times 10^{-3}$, $n = 16$) and mixed terrains ($\gamma = 3.0 \times 10^{-3}$, $n = 9$). The shape of a displacement profiles for faults is indicative of the mode of growth (i.e., restricted or unrestricted). Displacement plots show 52% of mare graben exhibit plateau-shaped profiles, indicating restricted fault growth, compared to 19% and 33% for highlands and mixed terrain graben, respectively. We attribute the large percentage of plateau-shaped profiles and the scatter in mare graben D_{max}/L data to restricted fault growth controlled by the local thickness of the mare basalts. Finally, we consider whether observationally based estimates of the distribution of mare basalt thicknesses is consistent with the width-depth relation of the inferred restricted graben.

1. Introduction

The characteristics of faults and fractures express the stress state, mechanical properties, and structure of planetary lithospheres in which they form. The most recent period of lunar tectonism is preserved in small lobate thrust fault scarps, the most common tectonic landforms on the farside (Watters et al., 2010, 2015). Lobate scarps are very young, some estimated to be active within the last 50–100 Ma (Watters et al., 2012; van der Bogert et al., 2018), and some may still be active (Watters et al., 2019). Larger scale tectonic landforms on the Moon are the nearside graben and wrinkle ridges, spatially related to lunar mare. Lunar graben may form as the result of different stress environments like those resulting from dike intrusion (e.g. Head and Wilson, 1993; Wilson and Head, 2017; Head & Wilson, 2017), or passive extension (e.g. Solomon and Head, 1979, 1980; Freed et al., 2001; Martin and Watters, 2021; Schleicher et al., 2019) from subsidence and flexure induced by loading of the lunar lithosphere by the mare basalts. In the presence of a mascon, subsidence and flexure results in passive extension, forming radial and concentric graben along basin margins, and contraction forming wrinkle ridges in the basin interiors (Melosh, 1978; Solomon and Head, 1979, 1980; Freed et al., 2001; Melosh et al., 2013). In non-mascon mare settings, subsidence and flexure may be modulated by the local strength and/or thickness of the elastic lithosphere (Martin and Watters, 2021; Schleicher et al., 2019; Watters, 2022). As such, the focus of this study are the ancient, large, mare proximal graben, rather than the recently formed (<50 myr) small graben concentrated on the back limb of lobate scarps (Watters et al., 2012).

The early onset of thermal expansion on the Moon likely induced graben formation (e.g. Andrews-Hannah et al., 2013; Sawada et al., 2016), however the best preserved graben are proximal to the nearside mare, forming prior to 3.6 Ga (Boyce, 1976; Lucchitta and Watkins, 1978; Hiesinger et al., 2000, 2003). Nearside graben typically exhibit a symmetric geometry in cross-section (often referred to as simple graben (Golombek, 1979; Golombek and McGill, 1983)). Lunar graben also generally lack offset or crosscut graben floors or walls that are characteristic of multiple episodes of extension, often referred to as complex graben (e.g Watters and Johnson, 2010). Unlike wrinkle ridges that are confined solely to the mare basalts, nearside graben are found in mare

* Corresponding author.
E-mail address: martines@si.edu (E.S. Martin).

https://doi.org/10.1016/j.icarus.2022.115215
Received 22 October 2021; Received in revised form 29 July 2022; Accepted 5 August 2022
Available online 15 August 2022

and highland terrains, as well as crosscutting both terrains (Fig. 1) (hereafter, referred to as mixed terrains). We can use fault displacement-length scaling to characterize lunar graben and assess whether their formation is influenced by the geologic setting (highlands, mare, or mixed) within which they form.

Displacement-length scaling, the relationship between the maximum displacement on a fault and its length, has been widely used to characterize terrestrial fault populations (e.g. Walsh and Watterson, 1988; Cowie and Scholz, 1992a, 1992b; Gillespie et al., 1992; Cartwright et al., 1995). The ratio of a fault's maximum displacement to its total length is influenced by the mechanical properties and tectonic setting of deformed crustal materials (Cowie and Scholz, 1992a, 1992b; Schultz et al., 2010). A fault's length and maximum displacement are related by a scaling factor γ where $D_{max} = \gamma L^n$, where $n = 1$ has been shown to be a good approximation to terrestrial and planetary fault populations (Cowie and Scholz, 1992a; Dawers et al., 1993;Watters et al., 2000; Schultz et al., 2010). The γ of a fault population is typically between $\sim 1.0 \times 10^{-1}$ and 1.0×10^{-3} and individual faults within a population may have widely different D_{max}/L ratios resulting from various influences. Variations in the D_{max}/L ratios (also referred to as scatter) in a fault population could result from fault linkages, interactions, overlap, or layering in the host rock (Schultz et al., 2010).

As a fault grows, it accumulates displacement and length proportionally according to the mechanical controls on the fault. Assuming a Linear Elastic Fracture Mechanics (LEFM) behavior (Pollard and Segall, 1987; Walsh and Watterson, 1988; Pollard and Fletcher, 2005), a plot of the displacement and length of an unrestricted fault will be semicircular to elliptical (Fig. 2a). Fault growth frequently occurs through the interaction and linkages of individual fault segments. As fault segments begin to interact, displacement where the faults overlap, often referred to as 'soft-link', will appear to deviate from the ideal elliptical shape (Fig. 2b). The two faults will begin to behave as one, the length will increase to the sum of the two individual faults, and the displacement profile will flatten or plateau. Plateau-shaped displacement profiles are also indicative of restricted fault growth, where faults are restricted from accumulating displacement as they grow in length. Fault restriction can occur when a developing fault encounters a mechanical discontinuity in the subsurface. Continued evolution of soft-linked fault segments will result in fully linked, or 'hard-link' faults, where the combined segments behave as a single fault with an elliptical displacement profile, consistent with unrestricted fault growth (Fig. 2c).

Previous studies of displacement-length scaling relationships of lunar graben were limited to lower resolution data returned prior to the Lunar Reconnaissance Orbiter (LRO) (Watters and Johnson, 2010), where the value of γ for the lunar graben population was reported to be 3.5×10^{-3}. Callihan and Klimczak (2019) examined a subset of the lunar graben population using high resolution imagery and altimetry data returned by LRO and report $\gamma = 2.3 \times 10^{-3}$. Here, we examine the displacement-length scaling relationships and displacement profiles of a subset of lunar graben within specific geologic terrains. We include graben forming in mare basalts, highlands, and mixed terrains (graben crosscutting both mare and highlands), to determine whether geologic setting has any control on graben formation on the lunar nearside. The displacement profiles are examined for evidence of restricted normal fault growth in the three settings. Additionally, we examine estimates of the thickness of the mare basalts and compare them with estimates of the depth of penetration of graben bounding normal faults.

2. Data collection

Two primary criteria were used to identify graben for this study: 1) those that are not heavily degraded and 2) those in which the full extent is discernable. Graben with en echelon segments were assessed to determine whether segments were fully-linked. Segments that were fully-linked were treated as a single graben; segments that were not fully-linked were treated as individual graben. Graben within floor fractured craters were not included, as the focus of this work is on nearside graben associated directly with the mare. All graben have experienced some degree of degradation including overlying impacts and emplacement of ejecta. Therefore the best preserved graben were chosen because they provide the most accurate measure of the structural relief and allow the most accurate estimate of the maximum displacement and the displacement along their length. A graben was deemed satisfactorily preserved if both rims were visible, and the presence of superposed impacts and ejecta emplacement did not obscure large portions of the normal faults. Additionally, graben were only selected if both terminuses were detectable to ensure an accurate measurement of total length. A total of fifty graben were selected for analysis (Fig. 3).

2.1. Maximum displacement

The throw on each of the two graben bounding normal faults were measured at 1 km intervals using Lunar Orbitar Laser Altimeter/SELenological and ENngineering Explorer gridded data (Barker et al., 2016).

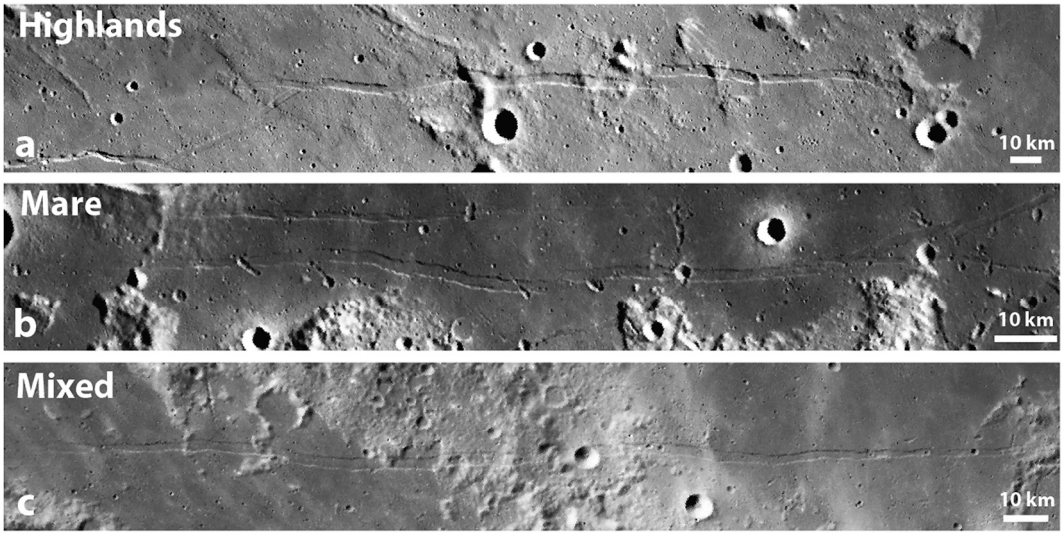

Fig. 1. Lunar graben within three terrain types, (a) highlands (centered at 6.61°N, 13.11°E), (b) mare (centered at −0.49°N, 22.41°E), (c) and a combination of the two referred to herein as mixed terrain (centered at −30.58°N, −21.78°E). Graben on the moon are generally symmetrical in their cross section, with flat floors bound by antithetic normal faults indicative of extension localized around nearside mare.

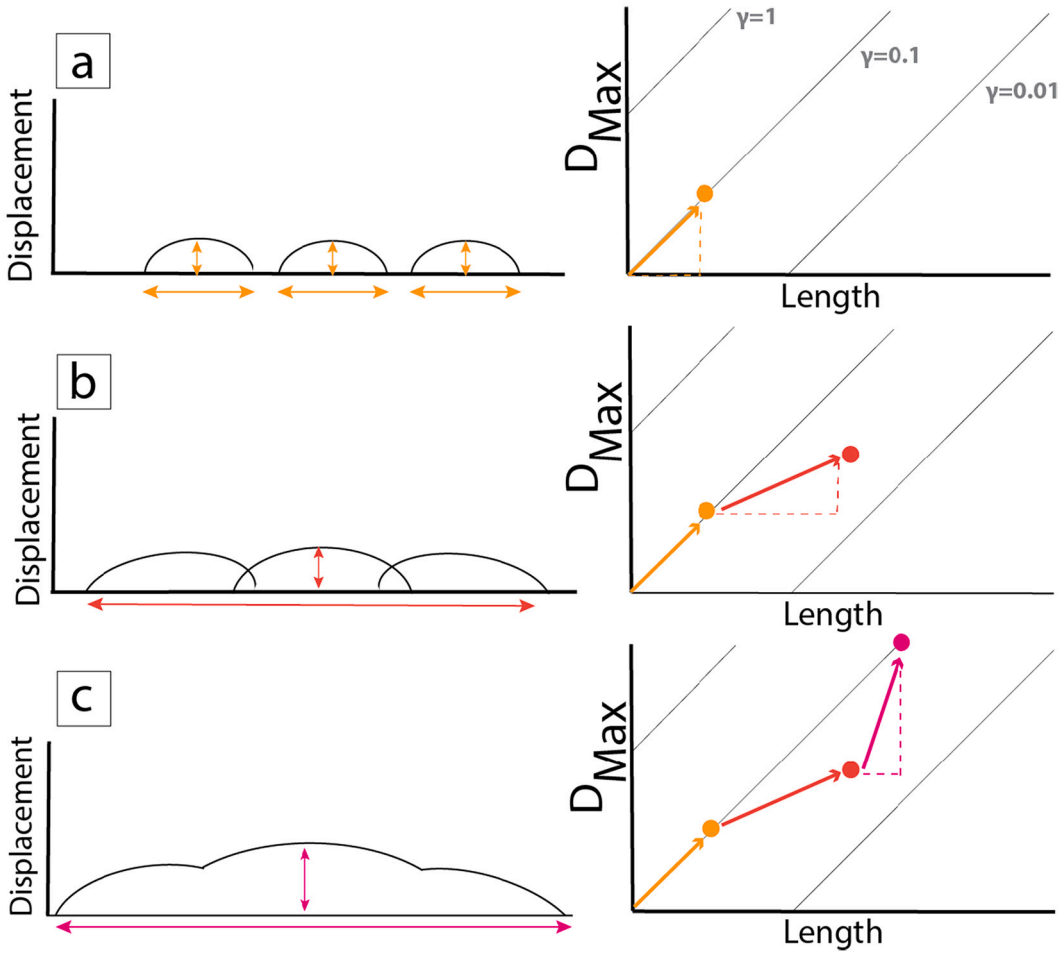

Fig. 2. Displacement evolution models. (a) As individual, unrestricted faults experience growth, their displacement profiles will be elliptical in shape. (b) As individual faults begin to interact and link, the combined displacement profile will flatten. If an individual fault encounters a restriction as it grows, it will continue to accumulate length with limited vertical displacement, also producing a plateau-shaped displacement profile. (c) As the faults fully link, they will grow as a single fault and the displacement profile will return to an elliptical shape. Plots after Schultz et al. (2010) and Fossen (2016).

Throw was determined by measuring the minimum and maximum elevation on each fault resulting in over 20,000 elevation measurements collected for this study. Displacement was inferred from throw assuming an average fault dip of 60°, assuming lunar graben are best characterized by a simple graben geometry (normal faults converge to a common point at depth). A displacement profile (Fig. 4) was created for each of the bounding normal faults to assess which of the two faults preserved the greatest displacement. Displacement profiles provide a robust means to determine a fault's maximum displacement and its location along the fault because D_{max} will not always occur at the fault-length midpoint. Models for fault geometries (i.e., Linear Elastic Fracture Mechanics (LEFM), post-yield fracture mechanics, or symmetric linear stress distribution, (see Schultz et al., 2010)) predict an unrestricted fault should achieve its maximum displacement near the midpoint of its length and zero displacement at the fault tips. The D_{max} assigned to each graben was determined by identifying the normal fault with the greatest displacement. We assume that degradation has removed some structural relief, thus the preserved relief at any point along the fault is a minimum including the estimate of maximum displacement. At locations along a graben where an overlying crater or ejecta obscured fault scarp relief, displacement data was not recorded.

2.2. Total length

An inaccurate estimate of fault length will result in an inaccurate D_{max}/L ratio. Fault degradation, superposed impact craters, illumination geometry, and fault segmentation all play a role in potentially complicating an accurate measurement of the fault length. We measured the relief beyond the discernable fault tips to ensure there was no unaccounted for structural relief. This technique ensured the full length of each fault from tip-to-tip was captured by identifying where displacement falls to zero (Fig. 4).

2.3. Displacement plot shape

The shape of a displacement profile can be indicative of unrestricted or restricted fault growth. LEFM theory predicts that unrestricted fault growth will produce an elliptically-shaped displacement profile. Restricted fault growth, where the fault is not free to extend vertically as it increases in length horizontally, can produce a flat- or plateau-shaped displacement profile (e.g. Soliva et al., 2005, 2006). A plateau-shaped displacement profile will also be produced by faults undergoing linkage (Fig. 2). Therefore, classifying the shape of displacement profiles is an important tool for identifying the mode of fault growth (i.e., restricted or unrestricted). Furthermore, the measurement of fault displacements within each profile generated in this study (Fig. 5) can be variable over short distances, making it difficult to characterize the overall shapes of the profiles. To more accurately characterize the displacement shapes, convex hulls were fit to each plot (Fig. 5). Convex hull fits are a means of representing the dominant shape of a distribution of points, avoiding potential errors introduced by methods such as a Fourier transform (e.g Atkins et al., 2021). To establish a statistical basis

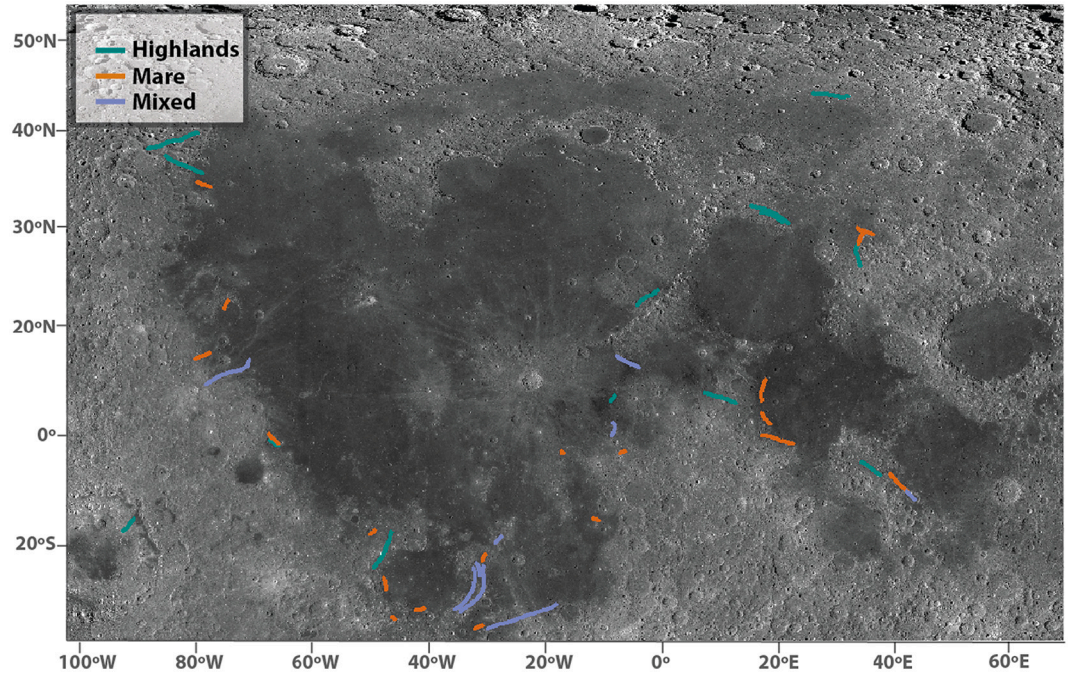

Fig. 3. Distribution of 50 selected nearside graben examined in this study color coded by setting (e.g., mare, highlands, or mixed mare-highlands terrains). Basemap is from the Lunar Reconnaissance Orbiter Camera Wide Angle Camera (WAC) (e.g. Speyerer et al., 2011).

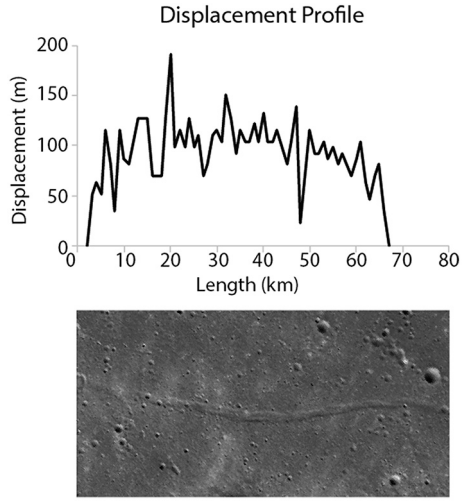

Fig. 4. An example graben displacement profile used to identify a graben's length and maximum displacement (D_{max}). At locations along graben where significant degredation affects robust measurements of throw, displacement was not recorded.

for classifying the shape of a displacement profile, we use the coefficient of variation (the ratio of the mean to the standard deviation) of all non-zero points in the convex hull fit. A plateau-shaped profile is one in which this ratio is generally $\geq$2.3 and an elliptical-shaped profile has a ratio generally <2.3 (see Appendix A).

3. Results

Of the 50 graben identified for this study (Fig. 3), 16 were within the highlands, 25 within mare basalts, and 9 were identified as mixed (within both highlands and mare) (Table 1). Mare terrains were identified using the mare basalt map from Nelson et al. (2014). Thirty-one of the 50 graben were found to have displacement profiles classified as elliptical-shaped, with 19 plateau-shaped (Fig. 5). Thirteen of the 25 graben in the mare have plateau-shaped profiles, a higher percentage than in either the highlands or mixed terrains. By contrast, only 3 of the 16 profiles of graben in the highlands are classified as plateau-shaped (see Appendix B).

Convex hull fits generalize the displacement profiles of the examined lunar graben. The high degree of scatter in many of the displacement profiles is at least partially due to the degradation state of the selected graben. Thus, outliers are expected (Table 2) and occur where convex hulls classified as elliptical, appear more plateau-shaped, and vice versa (see Appendix B). Excluding outlier graben has a negligible effect on the scaling factor of each fault population, and their resulting scatter. Furthermore, mare graben would still maintain the highest proportion of plateau-shaped displacement profiles relative to the other populations of graben.

The D_{max}/L relations were evaluated for normal faults examined in each of the three geologic settings. Values of γ were determined by a least squares fit to the D_{max}/L data for each sample graben population (Fig. 7). The γ value for graben in the highlands is $\sim 6.3 \times 10^{-3}$, $\sim 4.9 \times 10^{-3}$ for graben in the mare, and $\sim 3.0 \times 10^{-3}$ for graben in the mixed setting (Fig. 5, Table 1). Each graben population shows some scatter, quantified by the correlation coefficient R^2 (Fig. 7) for each least squares fit. The greatest amount of scatter and the lowest R^2 of $\sim$0.58 is found in the population of mare graben. The highlands and the mixed setting graben populations have the highest R^2 values at $\sim$0.77 and thus the least scatter.

4. Discussion

Lunar graben fall in the lower range of values of γ found for terrestrial normal faults (1.0×10^{-1} to 1.0×10^{-3}) (Watters and Johnson, 2010; Callihan and Klimczak, 2019), consistent with values of γ reported here (Fig. 8). Rheology can play a role in variations in γ of a fault population, however, the contrast in strain regime between Earth and one-plate lithosphere planetary bodies like the Moon is a key factor in accounting for the differences. Furthermore, the presence of liquid water likely acts to lubricate terrestrial faults resulting in higher values of γ

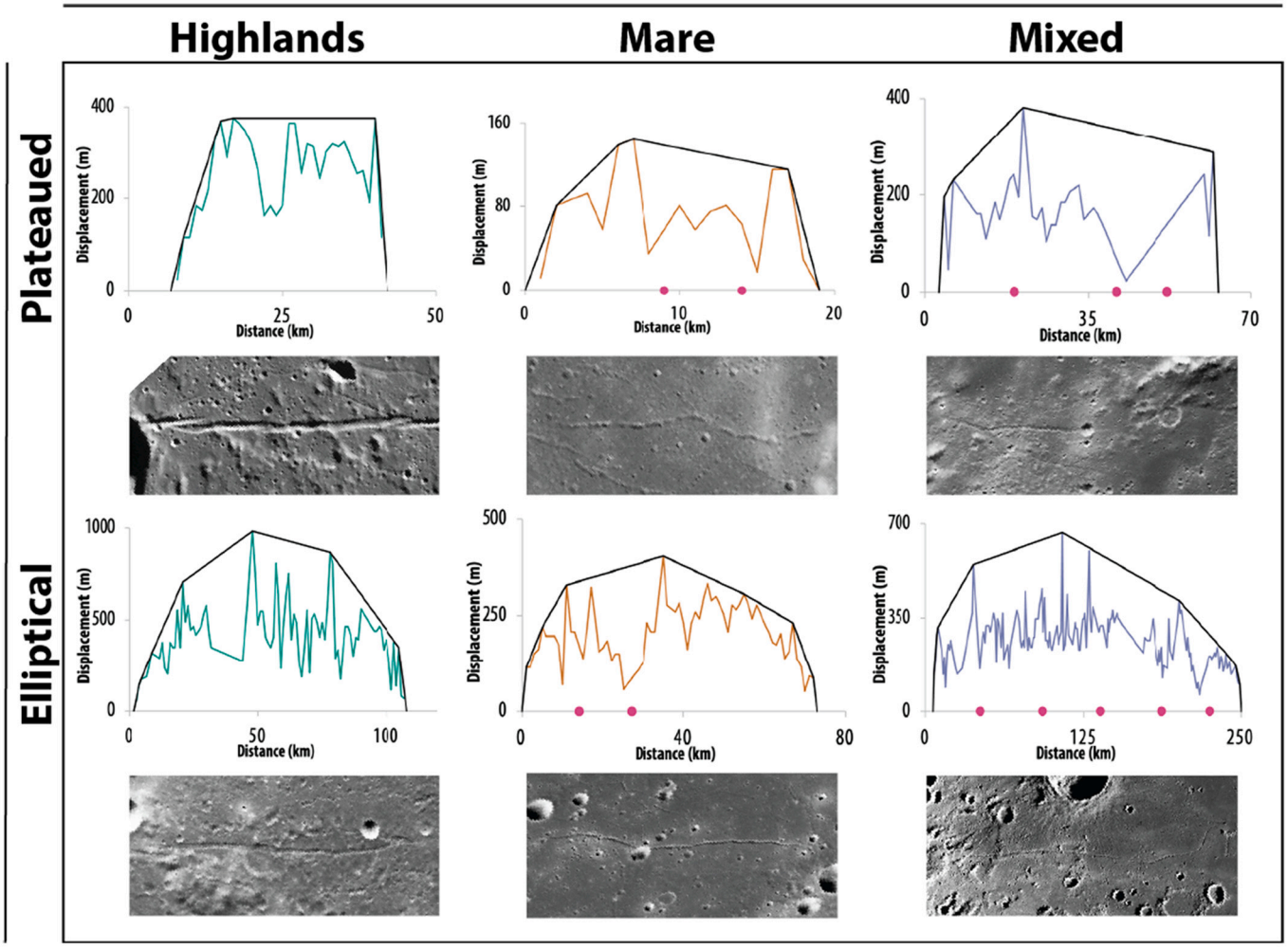

Fig. 5. A selection of elliptical- and plateau-shaped displacement plots for graben within each terrain (highlands, mare, mixed) identified for this work. Each displacement plot is accompanied by their associated convex hull fits (black lines). Pink points on the x-axis are the locations of segment intersections along the length of the fault (see Fig. 9). Displacement profiles are classified as plateau-shaped if the coefficient of variation (ratio of the mean to the standard deviation) of the non-zero points of the convex hull fit is $\geq$2.3. Here, the ratios are 2.4, 4.2, and 2.7 respectively for plateaued graben in the highlands, mare, and mixed terrains. The ratios are 1.2, 2.1, and 1.7 for elliptical graben in the highlands, mare, and mixed terrains respectively. See Appendix B for displacement profiles and convex hulls for all 50 graben in the population of graben selected for this work.

Table 1
Population and percentages of our sample of lunar graben with plateau- or elliptical-shaped displacement profiles in three geological settings: highlands, mare, and mixed terrains.

	Total	Plateau	Elliptical	%Plateau	%Elliptical	γ	R^2
Highlands	16	3	13	19%	81%	6.3×10^{-3}	0.77
Mare	25	13	12	52%	48%	4.9×10^{-3}	0.58
Mixed	9	3	6	33.3%	66.6%	3.0×10^{-3}	0.77

compared to populations of similar faults on the Moon and Mercury (Watters et al., 2000; Watters and Johnson, 2010).

While values of γ for lunar graben populations fit within an expected range for normal faults on terrestrial bodies, the high-scatter in D_{max}/L ratios of mare graben relative to highland graben may be an expression of the difference in the geologic setting. Scatter in D_{max}/L ratios of mare graben could be attributed to the number of fault segments that may have ceased development at different stages in the evolution of the fault linkages (e.g., Fig. 2). The stage of development of fault linkages can also add variability to the shape of displacement profiles of the graben normal faults (Fig. 2). In an analysis of fault segments, the number of segments was determined by identifying en echelon steps or large variations in fault azimuth along graben strike. While the mare graben appear to have a greater number of relatively short graben segments overall, the general distribution of each sample graben population are similar with few segments over 100 km long, and most segments 10–70 km in length (Fig. 9). Thus, it is concluded that the number of fault segments does not significantly influence the scatter in the D_{max}/L ratios or the shape of the displacement profiles (Fig. 5–7). We suggest the scatter in the D_{max}/L ratios of normal faults in the lunar mare is the result of restricted growth. This is consistent with a subset of lunar graben previously identified as having plateau-shaped displacement profiles also attributed to mechanical restriction (Callihan and Klimczak, 2019).

The near surface highlands crust is best characterized as a mechanically isotropic megaregolith. The high percentage of elliptical-shaped displacement profiles (Table 1) of highlands and mixed graben

Table 2
Location information for each selected graben as well as geological context, maximum displacement (D_{max}), length, and displacement-length ratio (D_{max}/L). Data outliers are identified by '*'. A displacement profile each graben can be found in Appendix B.

	ID	Center Lat (°N)	Center Long (°E)	D_{max} (m)	Length(km)	D_{max}/L
Highlands	1	-0.57	-64.55	375	33	$1.14x10^{-2}$
	2	-5.07	37.68	663	96	$6.9x10^{-3}$
	3*	6.76	-6.38	473	35	$1.4x10^{-2}$
	4	58.61	30.77	230	174	$1.3x10^{-3}$
	5	-1.14	-63.85	635	27	$2.35x10^{-2}$
	6	46.48	-79.49	692	185	$3.7x10^{-3}$
	7	-17.82	-44.74	981	104	$9.43x10^{-3}$
	8	24.20	-0.57	1154	136	$8.5x10^{-3}$
	9	-14.78	-88.85	837	86	$9.7x10^{-3}$
	10	38.56	20.64	837	197	$4.2x10^{-3}$
	11	50.63	-81.36	1039	198	$5.2x10^{-3}$
	12*	-20.77	-46.14	635	93	$6.83x10^{-3}$
	13	38.06	20.81	981	119	$8.2x10^{-3}$
	14	32.52	35.09	692	44	$1.57x10^{-2}$
	15	6.96	11.99	2026	165	$1.23x10^{-2}$
	16	30.70	35.42	635	67	$9.48x10^{-3}$
Mare	17	13.95	-76.36	172	85	$2.0x10^{-3}$
	18	-16.02	-47.34	155	32	$4.8x10^{-3}$
	19	-24.82	-45.23	669	53	$1.3x10^{-2}$
	20	-6.28	41.18	115	15	$7.67x10^{-3}$
	21	-30.65	-43.80	139	19	$7.3x10^{-3}$
	22	-2.34	-14.95	144	19	$7.6x10^{-3}$
	23	-13.81	-9.25	323	35	$9.2x10^{-3}$
	24	-2.35	-4.68	392	29	$1.35x10^{-2}$
	25	35.81	35.48	51	10	$5.10x10^{-3}$
	26	3.26	19.74	190	63	$3.02x10^{-3}$
	27	-32.20	-29.41	121	49	$2.5x10^{-3}$
	28	33.47	35.53	300	17	$1.76x10^{-2}$
	29	22.91	-72.38	167	46	$3.6x10^{-3}$
	30	-20.31	-28.51	288	54	$5.3x10^{-3}$
	31	-2.43	-15.11	75	12	$6.25x10^{-3}$
	32	-0.13	-64.29	1247	73	$1.7x10^{-2}$
	33	43.17	-76.10	404	72	$5.6x10^{-3}$
	34	-29.35	-39.38	207	47	$4.4x10^{-3}$
	35	-0.74	23.49	548	54	$1.01x10^{-2}$
	36	8.18	19.02	173	116	$1.5x10^{-3}$
	37*	-7.80	42.57	352	105	$3.35x10^{-3}$
	38	33.79	35.60	173	11	$1.57x10^{-2}$
	39	35.19	36.84	300	80	$3.75x10^{-3}$
	40	0.14	20.95	369	105	$3.51x10^{-3}$
	41	34.68	36.06	207	55	$3.76x10^{-3}$
Mixed	42	-30.59	-21.80	635	297	$2.1x10^{-3}$
	43	1.62	-6.11	381	66	$5.8x10^{-3}$
	44*	-17.25	-25.86	288	38	$7.58x10^{-3}$
	45	-9.76	44.50	635	52	$1.22x10^{-2}$
	46	12.90	-3.88	606	126	$4.8x10^{-3}$
	47	-22.45	-29.29	652	61	$1.1x10^{-2}$
	48	-26.28	-30.60	1039	233	$4.5x10^{-3}$
	49	-26.53	-28.94	519	275	$1.9x10^{-3}$
	50	11.12	-71.88	669	250	$2.7x10^{-3}$

suggests that normal fault growth in these settings is largely unrestricted. We interpret the unrestricted growth as an indication of the homogeneity of the mechanical properties of the lunar highlands. Based on Gravity Recovery and Interior Laboratory (GRAIL) data, a bulk density of 2550 kg m^{-3} suggests a pervasively fractured and highly porous lunar crust (Wieczorek et al., 2013). The large percentage of elliptical-shaped displacement profiles in the mixed highland-mare setting (Table 1), suggests that the mechanical properties of the highlands have the greater influence on normal fault growth in these locations. It is interesting to note that γ for mixed setting graben is similar to mare graben but with much less scatter in the D_{max}/L data. Other sources of scatter in D_{max}/L data may result from factors such as rock property variations, and error in determining maximum displacement and total fault length (Cartwright et al., 1995, 1996; Cowie, 1998; Dawers and Anders, 1995; Wojtal, 1996; Schultz, 1999).

If the high percentage of plateau-shaped displacement profiles for lunar mare graben are indicative of restricted fault growth, then fault restriction likely results from the mechanical discontinuity between the mare basalt sequence and the basin floor material. A mechanical discontinuity could limit the accumulation of vertical displacement as normal faults increase in length, resulting in a plateau-shaped displacement distribution. Local variations in the depth of mechanical discontinuities are expected to restrict normal fault growth to different degrees. Fault restriction controlled by varying thicknesses of mare

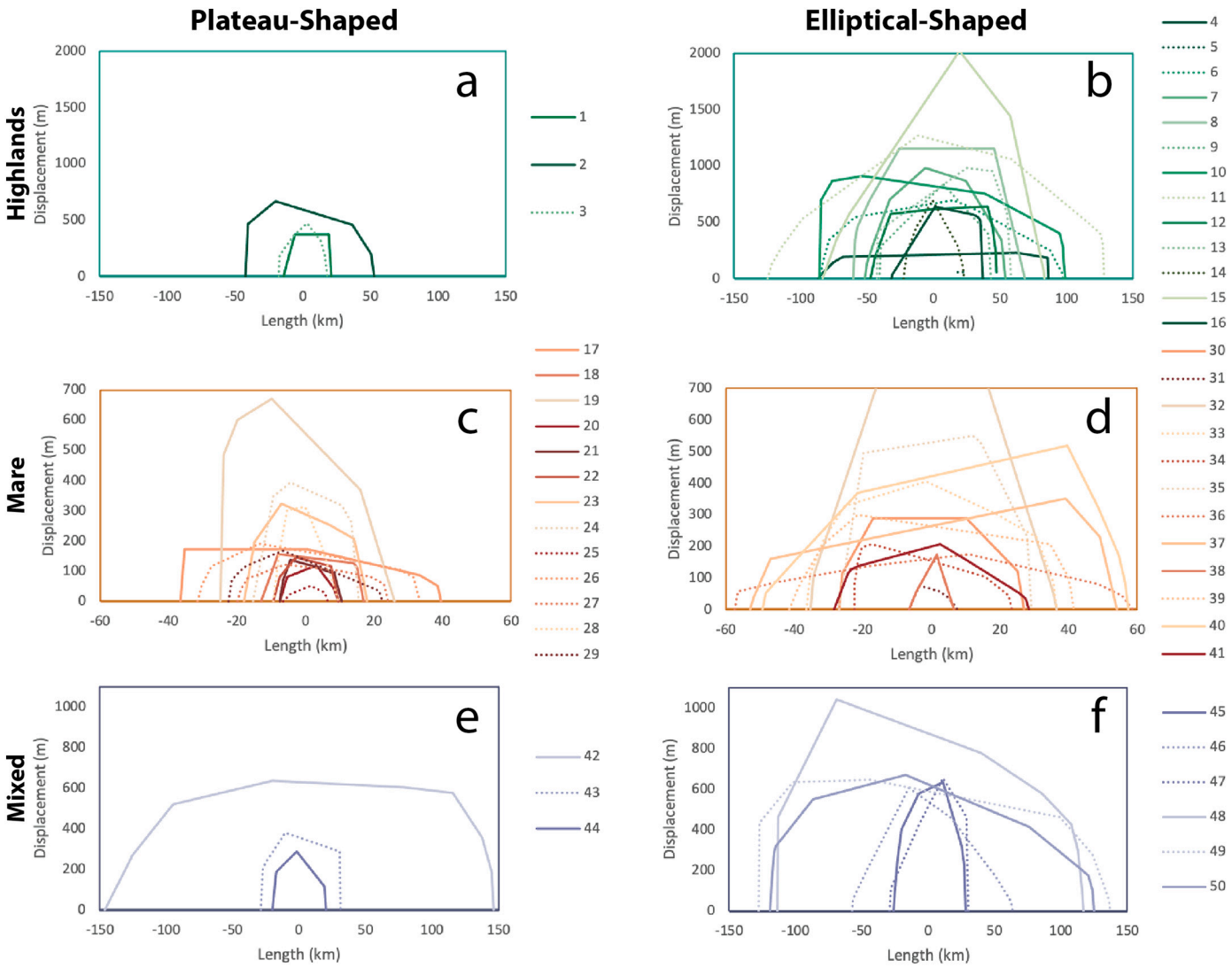

Fig. 6. Displacement profiles classified by shape of convex hull fits (elliptical- or plateau-shaped) for all 50 graben within the highlands (a,b), mare (c,d), and mixed terrains (e,f). Profile shape is defined by the coefficient of variation of non-zero points in the convex hull fits.

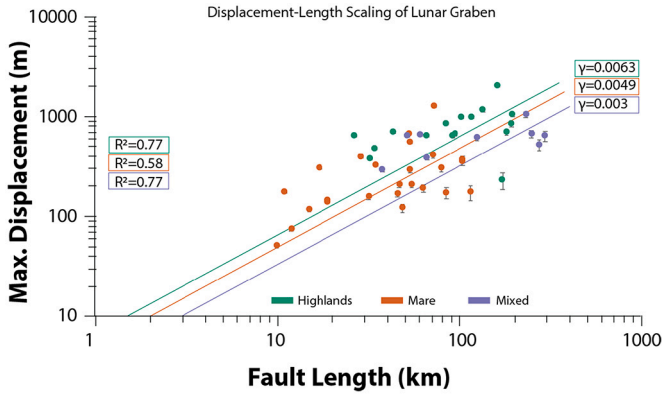

Fig. 7. Displacement-length scaling of three populations of lunar nearside graben selected in this study e.g. Fig. 3. Error bars represent ±25% of the D_{max} at each graben in our sample accounting for some unspecified amount of degradation of graben topography over time.

basalt sequences would be consistent with the greater scatter in D_{max}/L data and the lower correlation coefficient of the least squares fit for the sample mare graben population (Fig. 7). Although we interpret the greater scatter in the mare D_{max}/L fault population to be the result of variations in the total thickness of the mare basalts, the presence of layering in the sequences may also be a contributing factor.

Restricted mare graben may be an important indicator of the local thickness of the basalt sequence if the restricting mechanical discontinuity is the interface between mare basalts and basement rocks. The width of a restricted mare graben can be used to estimate the local basalt thickness. The simple graben model has antithetic normal faults intersecting at depth at a mechanical discontinuity (McGill, 1971; Golombek, 1979). The depth of intersection of the normal faults can be inferred from the graben width and an assumption about the fault-plane dip, generally assumed to be 60° (McGill, 1971; Golombek, 1979; Watters and Johnson, 2010). Because nearside graben are mostly confined to the margin of mare basins (excluding graben within floor fracture craters (e.g. Jozwiak et al., 2012, 2015), thickness estimates from graben widths are spatially restricted and may represent minimum thicknesses.

Previous methods for estimating variations in basalt thicknesses across the mare are based on partially buried (ghost) impact craters (300–400 m thick on average, up to 2 km) (DeHon, 1974, 1975, 1977, 1979; DeHon and Waskom, 1976; Horz, 1978), gravity data and topography (average 0.75 km on average, up to 1.62 km) (Gong et al., 2016), and buried lunar impact craters from GRAIL (1.5 km on average, up to 7 km) (Evans et al., 2016).

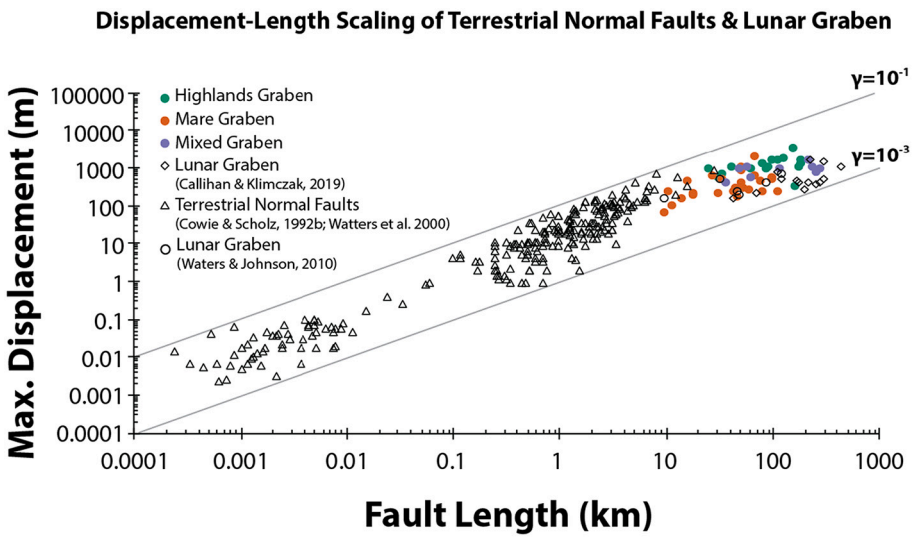

Fig. 8. Displacement-length scaling for terrestrial normal faults (Cowie and Scholz, 1992b) compared with lunar graben from this, and previous work (Watters and Johnson, 2010;Callihan and Klimczak, 2019).

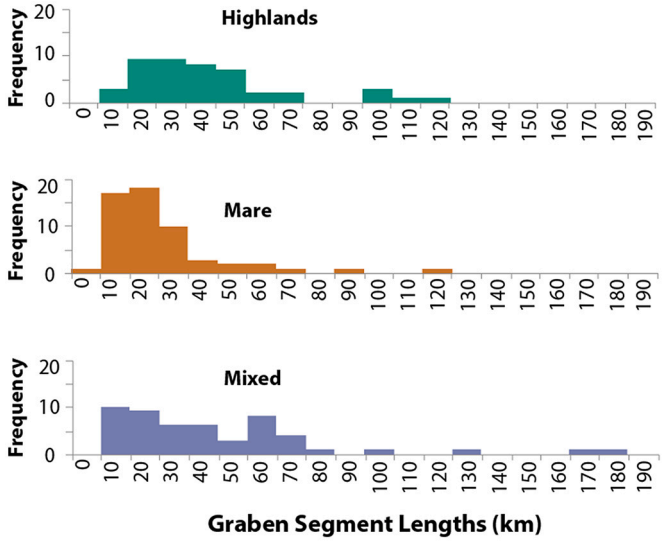

Fig. 9. Distribution of fault segment lengths within graben in lunar terrains. Mare graben have a slight trend towards more short fault segments overall, but the distribution of segment lengths are not significantly different between graben populations. The similarity in distribution of segment lengths suggests that no individual graben population is more segmented than another, and that graben segmentation is not influencing the shape of graben displacement profiles (Fig. 5).

The depth of faulting of mare graben normal faults is estimated to be 1 to 3 km for all mare graben examined (Fig. 10a), inferred from graben width. The mare graben normal faults classified as restricted extend to a depth of ~1–2 km, where the faults of those classified as unrestricted graben reach depths of ~3 km. The difference in depths between restricted and unrestricted mare graben might suggest that an initial restriction was eventually overcome by some graben, restoring the displacement profile to a more elliptical shape. Where mare graben are located near ghost craters, (DeHon, 1974; DeHon, 1975, 1977, 1979), basalt thicknesses are estimated to be under 1 km, two or more times thinner than the estimated restricted fault depth (Fig. 10a). Quasi-circular mass anomalies in the nearside mare revealed in GRAIL data are interpreted to be buried impact craters (Evans et al., 2016). There is good agreement between the inferred depth of faulting of the mare graben and estimates of basalt thicknesses from GRAIL buried craters (Fig. 10b). While some deviation occurs in southern Humorum, overall mare basalt thickness estimates from ghost craters (DeHon, 1974; DeHon, 1975, 1977, 1979) are consistently less than those derived from depth of normal faulting. It is worth noting that basalt thickness estimates from ghost craters were initially considered by some investigators to be too high (e.g. Horz, 1978), the more recent basalt thickness estimates derived from GRAIL suggest the opposite is true (Gong et al., 2016; Evans et al., 2016).

Many estimates of mare basalt thicknesses rely on the assumption about the shape of the mare prior to infilling. However, in the case of basins it is possible these basins were initially more pan-shaped than bowl-shape, meaning steeply sloping rims and flat-bottomed interiors (Watters and Konopliv, 2001). If the mare were initially pan-shaped, it would suggest some of the reported basalt thicknesses near the mare centers are overestimates (Fig. 10 see assumed partially buried craters). Furthermore, basalt thickness estimates would likely increase overall, as they would be more uniformly distributed across each mare. A pan-shaped basin would be consistent with the basalt sequences of up to 2 km thick near the basin rims inferred from the mare graben herein. While a selection bias exists because nearside graben are predominantly found on the perimeter of the mare, a pan-shaped basin would account for thick basalt sequences near the margins of mare basins.

5. Summary and conclusions

We present detailed observations of the displacement-length scaling of graben bounding normal faults around the nearside lunar mare to better understand the controls on their formation. The analysis reveals differences in the scatter of D_{max}/L ratios and the shape of displacement profiles of lunar graben in different geologic settings including highlands, mare, and mixed highland-mare terrains. We find greater scatter in the D_{max}/L data of mare graben, and find that it is likely not the result of immature fault linkages. It is concluded that many mare graben normal faults develop in an environment restricted by the local thickness of the mare basalts and the mechanical discontinuity at the base of the basalt sequences. Analysis of graben normal faults developed in the highlands and mixed settings show less evidence of restricted fault

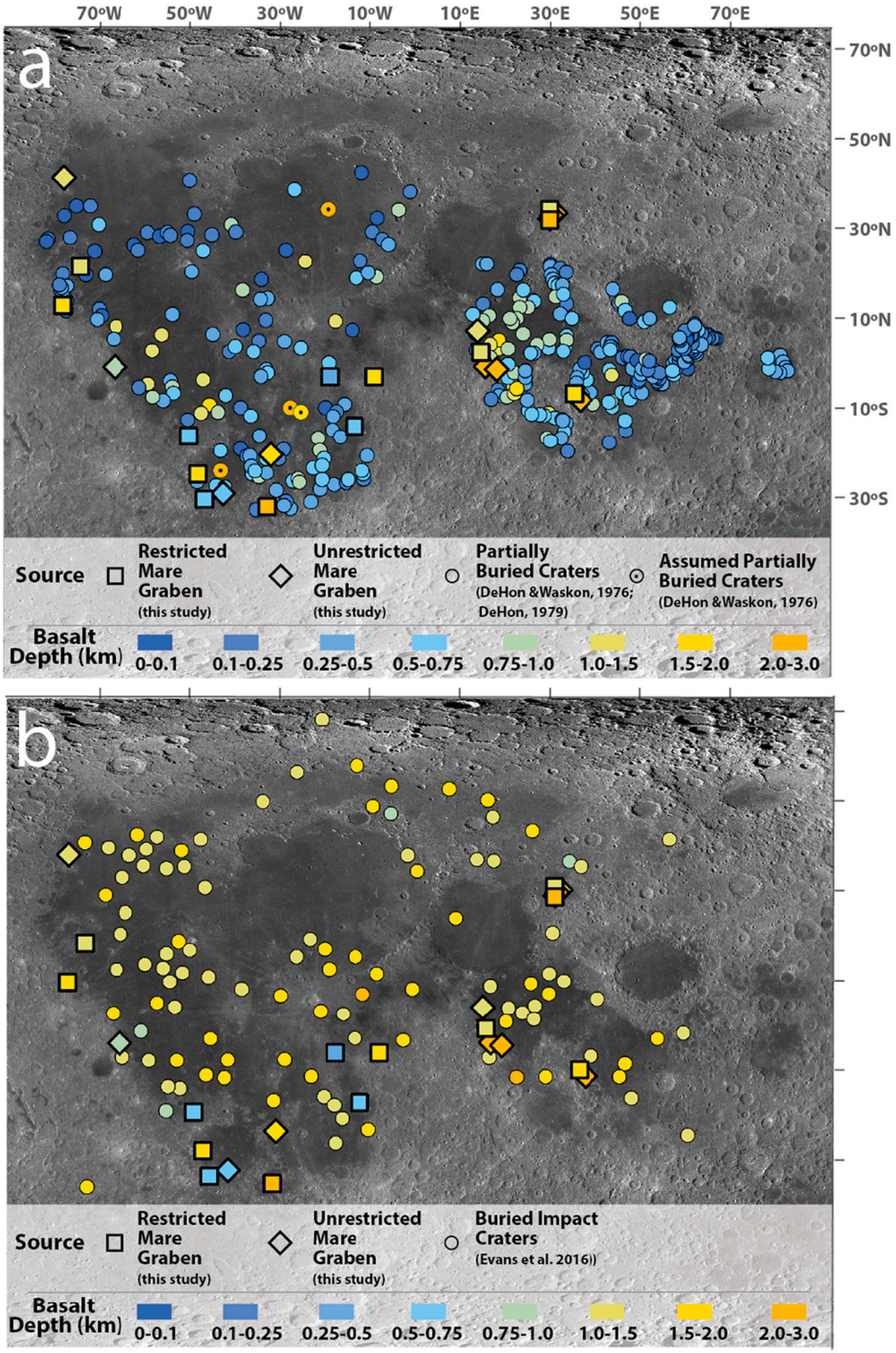

Fig. 10. Distribution of mare basalt thicknesses estimated using (a) ghost craters (circles) (DeHon, 1974; DeHon, 1975, 1977, 1979) and (b) buried lunar impact craters detected from GRAIL (Evans et al., 2016). Mare graben from this study plotted as squares (restricted graben) and diamonds (unrestricted graben).

growth likely due to the absence of shallow depth mechanical discontinuities. The results of this work provide new insight into the development of the nearside graben and the influence geologic setting had on their formation. The width-depth relation of the restricted mare graben suggests basalts up to 2 km thick, consistent with multiple studies based on observations from GRAIL.

Declaration of Competing Interest

None.

Data availability

Data contained within this publication are available on the Smithsonian FigShare Site (Smithsonian.figshare.com) or through the digital object identifier https://doi.org/10.25573/data.16832725. Supplemental files include high-resolution .png version of all figures, as well as data files in both .txt and .xlsx format for the data included in Figures 3, 5, 6, 7, 8, 9, 10 and Table 2. Also included are a data supplement to Figure 5 showing the displacement profiles and convex hulls of all 50 graben (Appendix B).

Acknowledgments

The authors would like to thank and acknowledge M. Callihan and two anonymous reviewers for their thoughtful comments that helped to significantly improve our manuscript. We acknowledge the hard work of the LROC team in data acquisition, distribution, and support. We also acknowledge the LRO engineers and technical support personnel. We thank Dr. Rene DeHon who provided original data sets that we digitized for this work. This work was supported by the LRO project and an ASU LROC contract to TRW.

Appendix A

The coefficient of variation is defined as the ratio of the mean and the standard deviation. The coefficient of variation (CV) is used as a statistical characterization the shape of the convex hull fits to the displacement profiles. The threshold is determined by assessing the CV values of convex hulls that represent endmembers of plateau- and elliptical-shaped displacement profiles. An idealized elliptical endmember is represented by a triangular-shaped displacement profile (Fig. A1a) with a CV of 1.4. An idealized plateau-shaped profile has a CV of 10.8. An idealized minimum plateau-shape profile, one with a shape roughly between the endmembers (Fig. A1c), has a CV of 2.3. Thus we characterize displacement profiles as plateau-shaped (CV $\geq$ 2.3) or elliptical-shaped (CV $<$ 2.3).

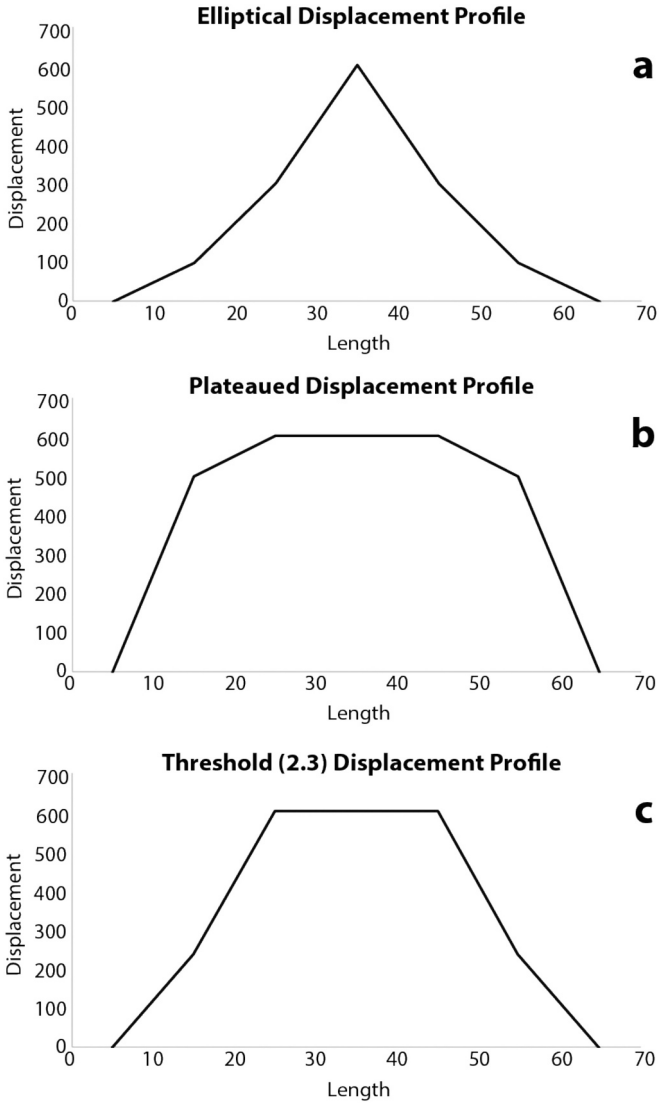

Fig. A1. Profiles highlighting endmembers for idealized elliptical- and (CV = 1.4) plateau-shaped (CV = 10.8) displacement profiles (a, b). The coefficient of variation was calculated for each plot. (**c**) Graphic representation of the threshold between elliptical- and plateau-shaped profiles. The threshold value of CV is 2.3.

Appendix B

The complete set of displacement profiles for all 50 graben within the sample population are shown. Each displacement profile is accompanied by their associated convex hull fit (black lines). Pink points on the x-axis are the locations of fault segments (e.g. Fig. 9). Graben are grouped by their geological terrain, either as highlands, mare, or mixed highlands-mare terrain. Each plot is also labeled with the coefficient of variation of all non-zero points in the convex hull fits indicating whether the profile is plateau-shaped ($\geq$ 2.3) or elliptical-shaped (<2.3).

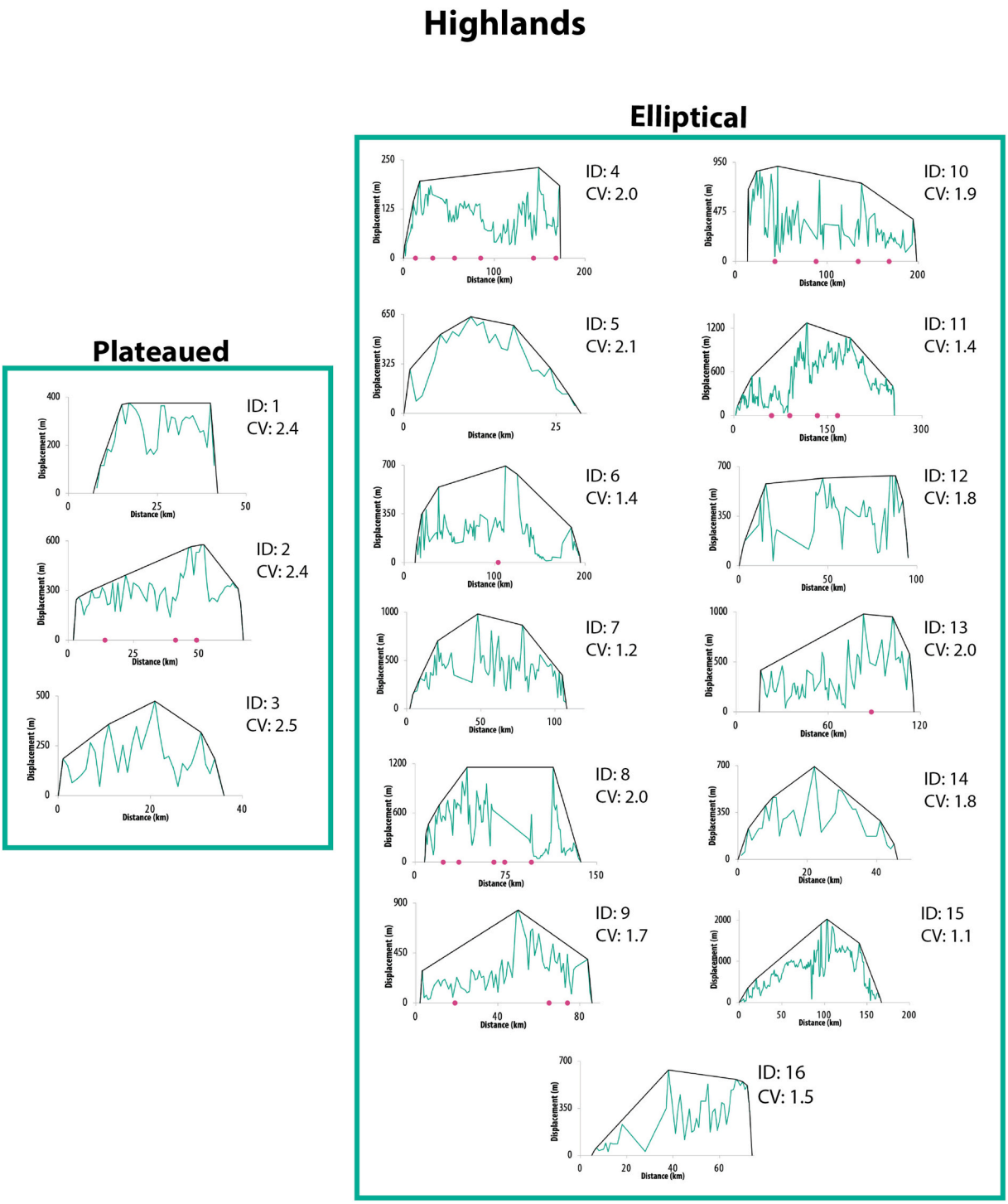

Fig. B1. Displacement profiles for all highlands graben in our sample population. A total of 16 highlands graben are included with 31% classified as restricted indicated by their plateau-shaped displacement profile and their CV value.

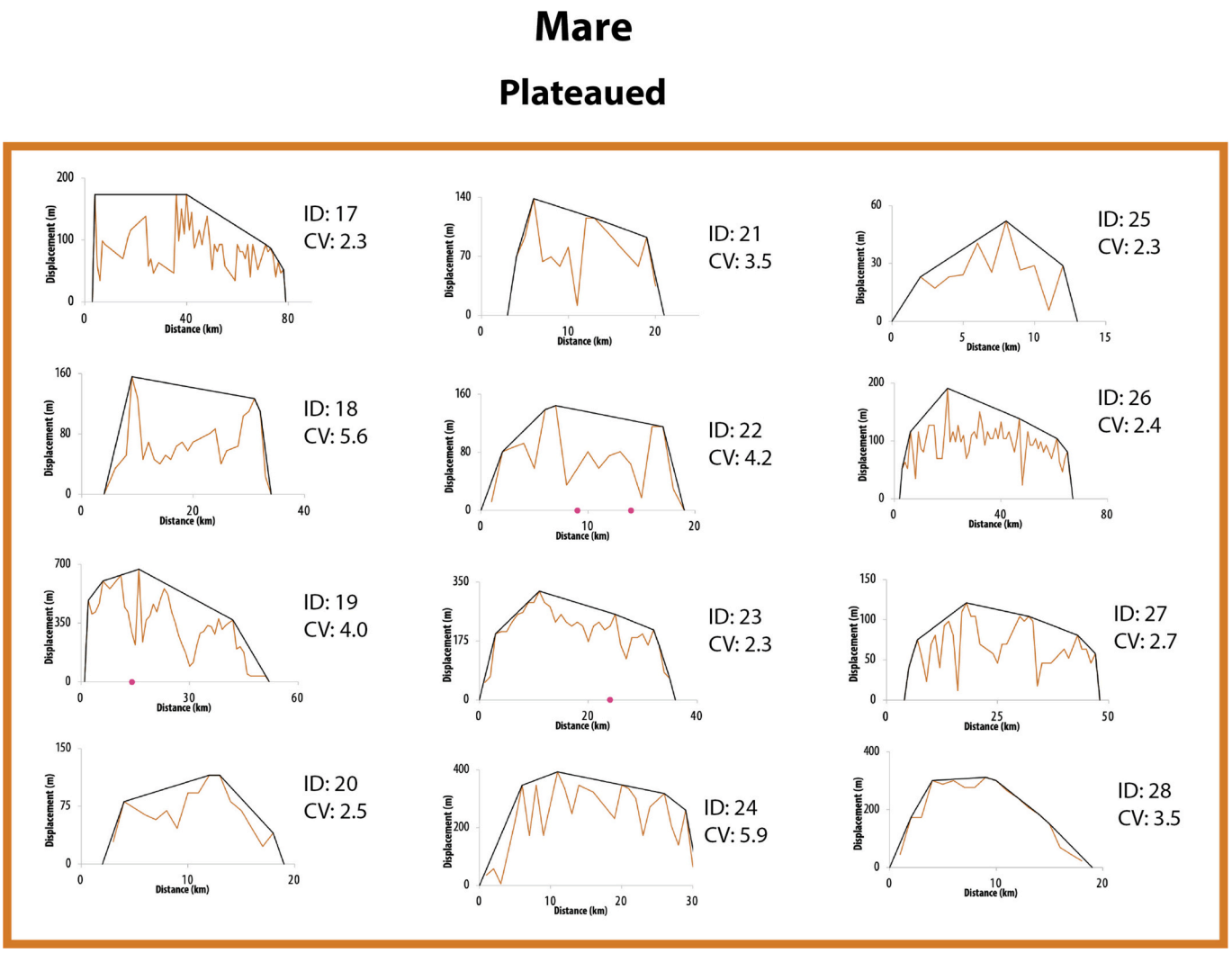

Fig. B2. Displacement profiles for all mare graben in our sample population. A total of 25 mare graben are included with 52% classified as restricted indicated by their plateau-shaped displacement profile and their CV value.

Elliptical

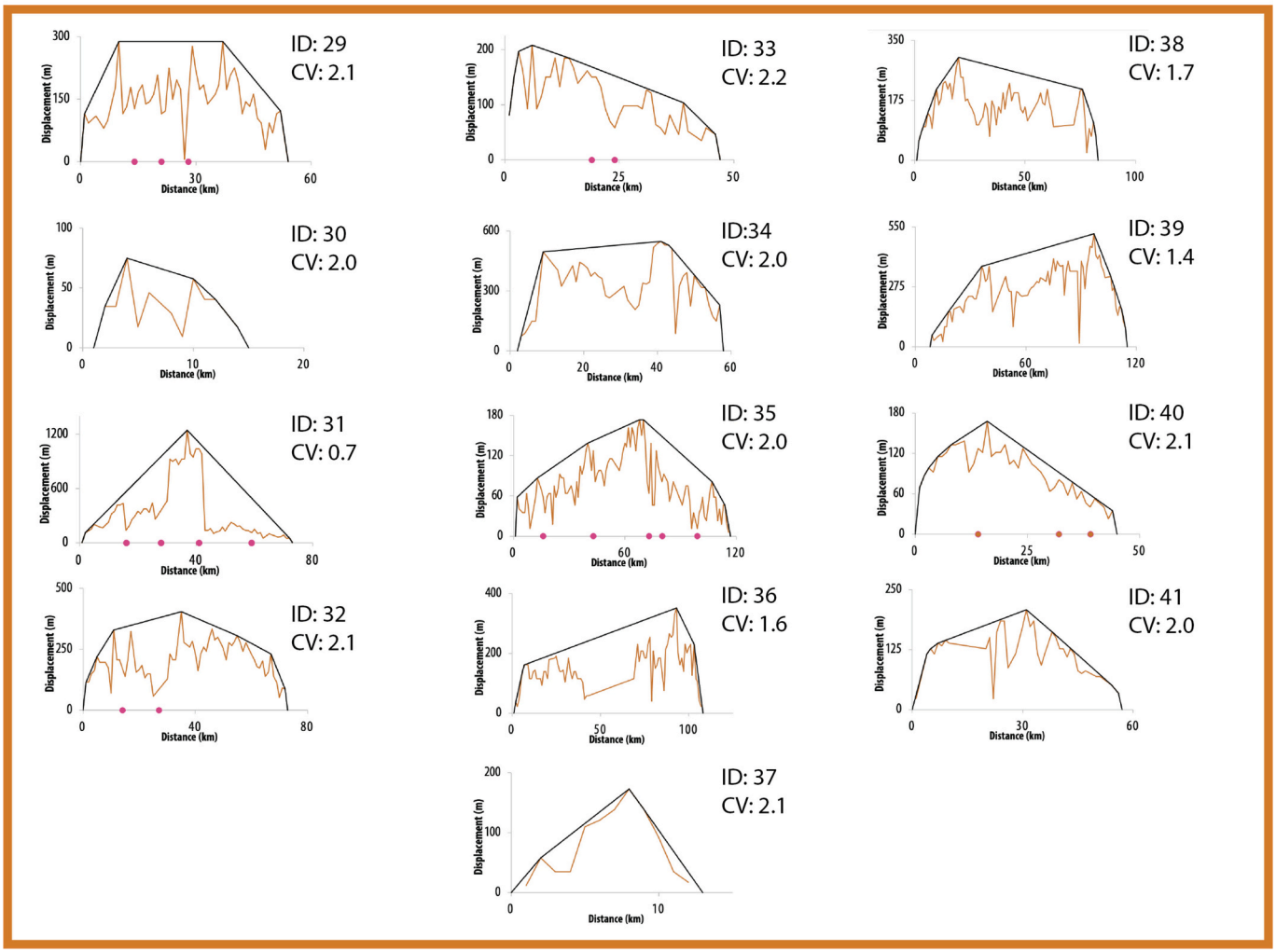

. (*continued*).

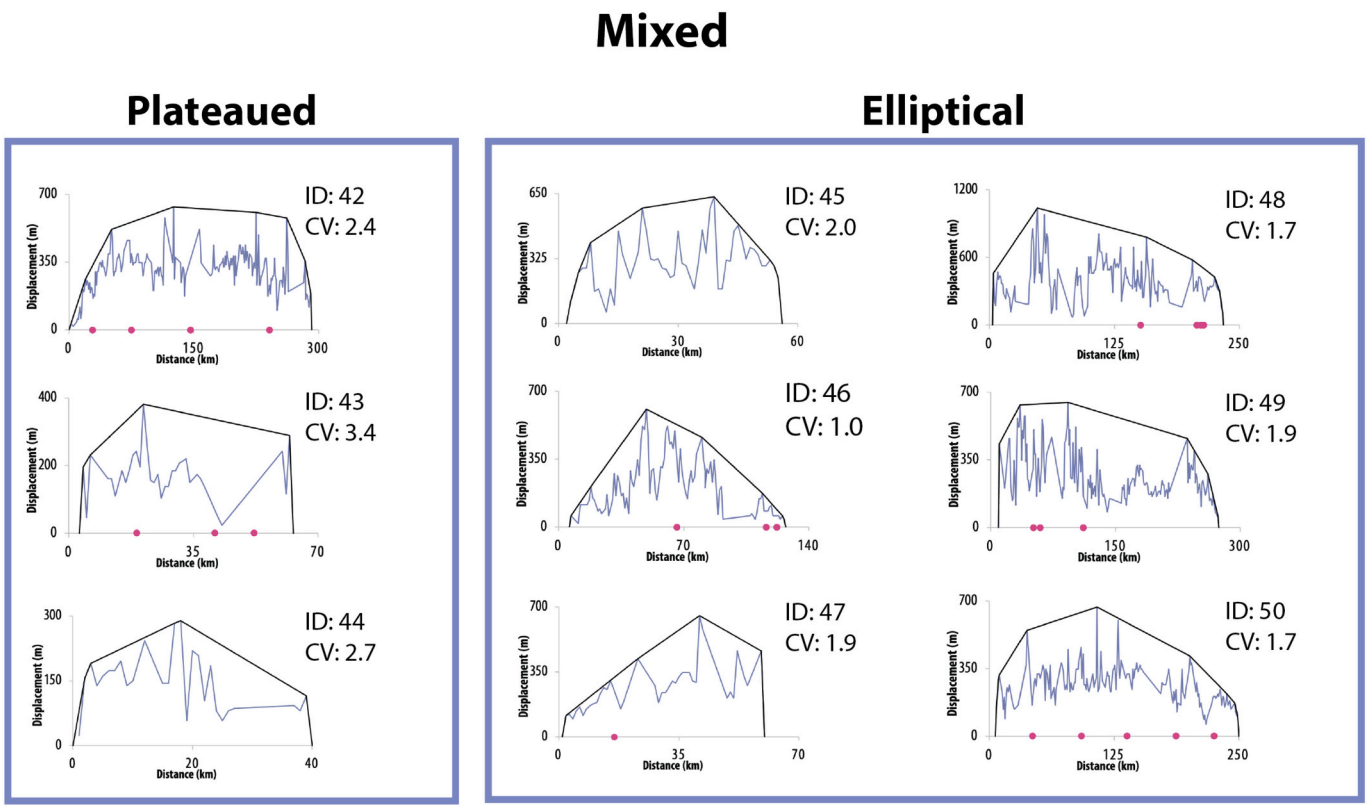

Fig. B3. Displacement profiles for all mixed highlands-mare graben in our sample population. A total of 9 mixed graben are included with 33.3% classified as restricted indicated by their plateau-shaped displacement profile and their CV value.

References

Andrews-Hannah, J.C., Asmar, A.W., Head, J.W., Kiefer, W.S., Konopliv, A.S., Lemoine, F.G., Matsuyama, I., Mazarico, E., McGovern, P.J., Melosh, H.J., Neumann, G.A., Nimmo, F., Phillips, R.J., Smith, D.E., Solomon, S.C., Taylor, G.J., Wieczorek, M.A., Williams, J.G., Zuber, M.T., 2013. Ancient igneous intrusions and early expansion of the moon revealed by GRAIL gravity Gradiometry. Science 339, 675–678. https://doi.org/10.1126/science.1231753.

Atkins, R.M., Byrne, P.K., Bohnenstiehl, Del Wayne R., 2021. Investigating morphometric characteristics of shortening structures across Mars. In: 52 LPSC, LPI Contrib. No. 2548. Abs. No. 1679.

Barker, M.K., Mazarico, E., Neumann, G.A., Zuber, M.T., Haruyama, J., Smith, D.E., 2016. A new lunar digital elevation model from the lunar orbiter laser altimeter and SELENE terrain camera. Icarus 273, 346–355. https://doi.org/10.1016/j.icarus.2015.07.039.

van der Bogert, C.H., Clark, J.D., Hiesinger, H., Banks, M.E., Watters, T.R., Robinson, M. S., 2018. How Old are Lunar Lobate Scarps? 1. SEISMIC Resetting of Crater Size-frequency Distributions. https://doi.org/10.1016/j.icarus.2018.01.019.

Boyce, J.M., 1976. Ages of flow units in the lunar nearside maria based on lunar orbiter IV photographs. Proc. Lunar Planet. Sci. Conf. 7, 2717–2728.

Callihan, M.B., Klimczak, C., 2019. Topographic expressions of lunar graben. Lithosphere 11, 294–305. https://doi.org/10.1130/L1025.1.

Cartwright, J.A., Trudgill, B.D., Mansfield, C.S., 1995. Fault growth by segment linkage: an explanation for scatter in maximum displacement and trace length data from the Canyonlands grabens of SE Utah. J. Struct. Geol. 17, 1319–1326. https://doi.org/10.1016/0191-8141(95)00033-A.

Cartwright, J.A., Mansfield, C.S., Trudgill, B.D., 1996. Fault growth by segment linkage. In: Buchanan, P.C., Nieuwland, D.A. (Eds.), Modern Developments in Structural Interpretation, vol. 99. Geol. Soc. Lond. Spec. Pub., pp. 163–177

Cowie, P.A., 1998. Normal fault growth in three-dimensions in continental and oceanic crust. In: Buck, W. Roger, Delaney, P.T., Karson, J.A., Lagabrielle, Y. (Eds.), Faulting and Magmatisim at Mid-ocean Ridges, Vol. 106. Geophysical Monograph, pp. 325–348. https://doi.org/10.1029/GM106p0325.

Cowie, Scholz, 1992a. Physical explanation for the displacement-length relationship of faults using a post-yield fracture mechanics model. J. Struct. Geol. 14, 1133–1148. https://doi.org/10.1016/0191-8141(92)90065-5.

Cowie, Scholz, 1992b. Displacement-length scaling relationship for faults: data synthesis and discussion. J. Struct. Geol. 14, 1149–1156. https://doi.org/10.1016/0191-8141(92)90066-6.

Dawers, N.H., Anders, M.H., 1995. Displacement-length scaling and fault linkage. J. Struct. Geol. 17, 607–614. https://doi.org/10.1016/0191-8141(94)00091-D.

Dawers, N.H., Anders, M.H., Scholz, C.H., 1993. Growth of normal faults: displacement-length scaling. Geology 21, 1107–1110.

DeHon, R.A., 1974. Thickness of mare material in the Tranquillitatis and Nectaris basins. Proc. Lunar Planet. Sci. Conf. 5, 53–59.

DeHon, R.A., 1975. Mare Spumans and Mare Undarum: Mare thickness and basin floor. Proc. Lunar Planet. Sci. Conf. 6, 2553–2561.

DeHon, R.A., 1977. Mare Humorum and Mare Nubium: basalt thickness and basin-forming history. Proc. Lunar Sci. Conf. 8, 633–641.

DeHon, R.A., 1979. Thickness of the western mare basalts. Proc. Lunar Planet. Sci. Conf. 10, 2935–2955.

DeHon, R.A., Waskom, J.D., 1976. Geologic structure of the eastern mare basins. Proc. Lunar Planet. Sci. Conf. 7, 2729–2746.

Evans, A.J., Soderblom, J.M., Andrews-Hanna, J.C., Solomon, S.C., Zuber, M.T., 2016. Identification of buried lunar impact craters from GRAIL data and implications for the nearside maria. Geophys. Res. Lett. 43, 2445–2455. https://doi.org/10.1002/2015GL067394.

Fossen, H., 2016. Structural Geology, 2nd edition. Cambridge University Press, Cambridge, UK, p. 211.

Freed, A.M., Melosh, H.J., Solomon, S.C., 2001. Tectonics of mason loading: resolution of the strike-slip faulting paradox. J. Geophys. Res. 106, 20603–20620. https://doi.org/10.1029/2000JE001347.

Gillespie, P.A., Walsh, J.J., Watterson, J., 1992. Limitations of dimension and displacement data from single faults and the consequences for data analysis and interpretation. J. Struct. Geol. 14, 1157–1172. https://doi.org/10.1016/0191-8141(92)90067-7.

Golombek, M.P., 1979. Structural analysis of lunar grabens and the shallow crustal structure of the moon. J. Geophs. Res 84, 4657–4666. https://doi.org/10.1029/JB084iB09p04657.

Golombek, M.P., McGill, G.E., 1983. Grabens, basin tectonics, and the maximum total expansion of the moon. J. Geophys. Res. 88, 3563–3578. https://doi.org/10.1029/JB088iB04p03563.

Gong, S., Wieczorek, M.A., Nimmo, F., Kiefer, W.S., Head, J.W., Huang, C., Smith, D.E., Zuber, M.T., 2016. Thicknesses of mare basalts on the moon from gravity and topography. J. Geophys. Res. 121, 854–870. https://doi.org/10.1002/2016JE005008.

Head III, J.W., Wilson, L., 1993. Lunar graben formation due to near-surface deformation accompanying dike emplacement. Planet. Space Sci. 41, 719–727. https://doi.org/10.1016/0032-0633(93)90114-H.

Head III, J.W., Wilson, L., 2017. Generation, ascent and eruption of magma on the moon: new insights into source depths, magma supply, intrusions and effusive/explosive

eruptions (part 2: predicted emplacement processes and observations). Icarus 283, 176–223. https://doi.org/10.1016/j.icarus.2016.05.031.
Hiesinger, H., Jaumann, R., Neukam, G., Head, J.W., 2000. Ages of mare basalts on the lunar nearside. J. Geophys. Res. 105, 29239–29276. https://doi.org/10.1029/2000JE001244.
Hiesinger, H., Head III, J.W., Wolf, W., Jaumann, R., Neukum, G., 2003. Ages and stratigraphy of Mare basalts in Oceanus Procellarum, Mare Nubium, Mare Congnitum, and Mare Insularum. J. Geophys. Res. 108 (E7), 5060. https://doi.org/10.1029/2002JE001985.
Horz, F., 1978. How thick are lunar mare basalts? Proc. Lunar Planet. Sci. Conf. 9, 3311–3331.
Jozwiak, L.M., Head, J.W., Wilsok, L., 2015. Lunar floor-fractured craters as magmatic intrusions: Geometry, modes of emplacement, associated tectonic and volcanic features, and implications for gravity anomalies. Icarus 248, 424–447. https://doi.org/10.1016/j.icarus.2014.10.052.
Jozwiak, L.M., Head, J.W., Zuber, M.T., Smith, D.E., Neumann, G.A., 2012. Lunar floor-fractured craters: classification, distribution, origin and implications for magmatism and shallow crustal structure. J. Geophys. Res. 117, E11005. https://doi.org/10.1029/2012JE004134.
Lucchitta, B.K., Watkins, J.A., 1978. Age of graben systems on the moon. Proc. Lunar Planet. Sci. Conf. 9, 3459–3472.
Martin, E.S., Watters, T.R., 2021. Topography of nearside mare graben: implications for dike-induced or passive extension formation. Icarus 354, 114039. https://doi.org/10.1016/j.icarus.2020.114039.
McGill, G.E., 1971. Attitude of fractures bounding straight and arcuate lunar rilles. Icarus 14, 53–58. https://doi.org/10.1016/0019-1035(71)90101-1.
Melosh, H.J., 1978. The tectonics of mascon loading. Proc. Lunar Planet. Sci. Conf. 9th, 3513–3525.
Melosh, H.J., Freed, A.M., Johnson, B.C., Blair, D.M., Andrews-Hanna, J.C., Neumann, G. A., Phillips, R.J., Smith, D.E., Solomon, S.C., Wieczorek, M.A., Zuber, M.T., 2013. The origin of lunar mascon basins. Science 340, 1552–1555. https://doi.org/10.1126/Science.1235768.
Nelson, D.M., Koeber, S.D., Daud, K., Robinson, M.S., Watters, T.R., Banks, M.E., Williams, N.R., 2014. Mapping lunar maria extents and lobate scarps using LROC image products. In: 45th LPSC, Abs. No. 2861.
Pollard, D.D., Fletcher, R.C., 2005. Fundamentals of Structural Geology. Cambridge University Press.
Pollard, D.D., Segall, P., 1987. Theoretical displacements and stresses near fractures in rock, with applications of faults, joints, veins, dikes, and solution surfaces. In: Atkinson, B.K. (Ed.), Fracture Mechanics of Rock. Academic Press, London, England, pp. 277–349.
Sawada, N., Morota, T., Kato, S., Ishihara, Y., Hiramatsu, Y., 2016. Constraints on timing and magnitude of early global expansion of the moon from topographic features in linear gravity anomaly areas. Geophys. Res. Lett. 43, 4865–4870. https://doi.org/10.1002/2016GL068966.
Schleicher, L.S., Watters, T.R., Martin, A.J., Banks, M.E., 2019. Wrinkle ridges on mercury and the moon within and outside of mascons. Icarus 331, 226–237. https://doi.org/10.1016/j.icarus.2019.04.013.
Schultz, R.A., 1999. Understanding the process of faulting: selected challenges and opportunities at the edge of the 21st century. J. Struct. Geol. 21, 985–993. https://doi.org/10.1016/S01918141(99)00025-5.
Schultz, R.A., Soliva, R., Okubo, C.H., M'ege, D., 2010. Fault populations. In: Thomas, R. (Ed.), Planetary Tectonics. Cambridge University Press, Watters & Richard A. Schulz, p. 457.
Soliva, R., Schultz, R.A., Benedicto, A., Soliva, R., 2005. Three-dimensional displacement-length scaling and maximum dimension of normal faults in layered rocks. Geophys. Res. Lett. 32, L16302. https://doi.org/10.1029/2005GL023007.
Soliva, R., Benedicto, A., Maerten, L., 2006. Spacing and linkage of confined normal faults: importance of mechanical thickness. J. Geophys. Res. 111, B01402. https://doi.org/10.1029/2004JB003507.
Solomon, S.C., Head, J.W., 1979. Vertical movement in mare basins: relation to mare emplacement, basin tectonics, and lunar thermal history. J. Geophys. Res. 84, 1667–1682. https://doi.org/10.1029/JB084iB04p01667.
Solomon, S.C., Head, J.W., 1980. Lunar mascon basins: lava filling, tectonics, and evolution of the lithosphere. Rev. Geophys. 18, 107–141. https://doi.org/10.1029/RG018i001p00107.
Speyerer, E.J., Robinson, M.S., Denevi, B.W., LROC Team, 2011. Lunar Reconnaissance Orbiter Camera Morphological Map of the Moon. In: 42nd Lunar and Planetary Science Conference Abs. No. 2387.
Walsh, J.J., Watterson, J., 1988. An analysis of the relationship between displacements and dimensions of faults. J. Struct. Geol. 10, 239–247. https://doi.org/10.1016/0191-8141(88)90057-0.
Watters, T.R., 2022. Lunar wrinkle ridges and the evolution of the nearside lithosphere. J. Geophys. Res. 127, e2021JE007058 https://doi.org/10.1029/2021JE007058.
Watters, T., Johnson, C., 2010. Lunar tectonics. In: Watters, T.R., Schultz, R.A. (Eds.), Planetary Tectonics. Cambridge University Press, New York, NY, pp. 121–182.
Watters, T.R., Konopliv, A.S., 2001. The topography and gravity of Mare Serenitatis: implications for subsidence of the mare surface. Planetary & Space Sci. 49, 743–748. https://doi.org/10.1016/S0032-0633(01)00007-1.
Watters, T.R., Schultz, R.A., Robinson, M.S., 2000. Displacement-length relations of thrust faults associated with lobate scarps on mercury and Mars: comparison with terrestrial faults. GRL 27, 3659–3662. https://doi.org/10.1029/2000GL011554.
Watters, T.R., Robinson, M.S., Beyer, R.A., Banks, M.E., Bell III, J.F., Pritchard, M.E., Hiesinger, H., van der Bogert, C.H., Thomas, P.C., Turtle, E.P., Williams, N.R., 2010. Evidence of recent thrust faulting on the moon revealed by the lunar reconnaissance orbiter camera. Science 329 (5994), 936–940. https://doi.org/10.1126/science.1189590.
Watters, T.R., Robinson, M.S., Banks, M.E., Tran, T., Denevi, B., 2012. Recent extensional tectonics on the moon revealed by the lunar reconnaissance orbiter camera. Nat. Geosci. 5, 181–185. https://doi.org/10.1038/ngeo1387.
Watters, T.R., Robinson, M.S., Collins, G.C., Banks, M.E., Daud, K., Williams, N.R., Selvans, M.S., 2015. Global thrust faulting on the moon and the influence of tidal stresses. Geology 43, 851–854. https://doi.org/10.1130/G37120.1.
Watters, T.R., Weber, R.C., Collins, G.C., Howley, I.J., Schmerr, N.C., Johnson, C.L., 2019. Shallow seismic activity and young thrust faults on the moon. Nat. Geosci. 12, 411–417. https://doi.org/10.1038/s41561-019-0362-2.
Wieczorek, M.A., Neumann, G.A., Nimmo, F., Kiefer, W.S., Taylor, G.J., Melosh, H.J., Phillips, R.J., Solomon, S.C., Andrews-Hanna, J.C., Asmar, S.W., Konopliv, A.S., Lemoine, F.G., Smith, D.E., Watkins, M.M., Williams, J.G., Zuber, M.T., 2013. The crust of the moon as seen by GRAIL. Science v. 339, 671–675. https://doi.org/10.1126/science.1231530.
Wilson, L., Head, J.W., 2017. Generation, ascent and eruption of magma on the moon: new insights into source depths, magma supply, intrusions and effusive/explosive eruptions (part 1: theory). Icarus 283, 146–175.
Wojtal, S.F., 1996. Changes in fault displacement populations correlated to linkage between faults. J. Struct. Geol. 18, 265–279. https://doi.org/10.1016/S0191-8141(96)80049-6.